Evaluation of cerebral cortex viscoelastic property estimation with nonlinear inversion magnetic resonance elastography

Lucy V. Hiscox[1], Matthew D.J. McGarry[2], Curtis L. Johnson[1]

[1]Department of Biomedical Engineering, University of Delaware; Newark, DE, USA

[2]Thayer School of Engineering, Dartmouth College; Hanover, NH, USA.

Competing interests: No competing interests to disclose.

Author contributions: LV Hiscox: Conceptualization, Methodology, Formal Analysis, Investigation, Writing – Original Draft, Visualization, MDJ McGarry: Data Curation, Software, Supervision, Writing – Review & Editing. CL Johnson: Conceptualization, Supervision, Funding Acquisition, Writing – Review & Editing.

Data availability: Simulated and inverted data from all experiments are available at:

www.github.com/mechneurolab.

Ethical statement: The study was approved by the Institutional Review Board of the University of Delaware and all participants provided written informed consent prior to participation. The research was conducted in accordance with the principles embodied in the Declaration of Helsinki and in accordance with local statutory requirements.

Abstract

Objective: Magnetic resonance elastography (MRE) of the brain has shown promise as a sensitive neuroimaging biomarker for neurodegenerative disorders; however, the accuracy of performing MRE of the cerebral cortex warrants investigation due to the unique challenges of studying thinner and more complex geometries.

Approach: A series of realistic, whole-brain simulation experiments are performed to examine the accuracy of MRE to measure the viscoelasticity (shear stiffness, μ, and damping ratio, ξ) of cortical structures predominantly effected in aging and neurodegeneration. Variations to MRE spatial resolution and the regularization of a nonlinear inversion (NLI) approach are examined.

Main results: Higher-resolution MRE displacement data (1.25 mm isotropic resolution) and NLI with a low soft prior regularization weighting provided minimal measurement error compared to other studied protocols. With the optimized protocol, an average error in μ and ξ was 3% and 11%, respectively, when compared with the known ground truth. Mid-line structures, as opposed to those on the cortical surface, generally display greater error. Varying model boundary conditions and reducing the thickness of the cortex by up to 0.67 mm (which is a realistic portrayal of neurodegenerative pathology) results in no loss in reconstruction accuracy.

Significance: These experiments establish quantitative guidelines for the accuracy expected of *in vivo* MRE of the cortex, with the proposed method providing valid MRE measures for future investigations into cortical viscoelasticity and relationships with health, cognition, and behavior.

Introduction

The biomechanics of biological tissue show a close relationship with tissue health and function, as evidenced through *ex vivo* analysis of tissue samples and the remarkable clinical success of palpation in disease detection. Once not thought to be possible, the mechanical properties of the brain can now be visualized non-invasively and *in vivo* through the advent of magnetic resonance elastography (MRE) (Manduca *et al.*, 2001; Muthupillai *et al.*, 1995). MRE shows considerable promise as an imaging biomarker of neurodegenerative diseases as the derived measurements relate to the underlying complexity and organization of the neural tissue microstructure (Guo *et al.*, 2019; Sack *et al.*, 2013) and have shown high sensitivity to a number of pathophysiological processes including Alzheimer's disease (Gerischer *et al.*, 2018; Hiscox, Johnson, McGarry, Marshall*, et al.*, 2020; Murphy *et al.*, 2011; Murphy *et al.*, 2015) and multiple sclerosis (Streitberger *et al.*, 2012; Wuerfel *et al.*, 2010), as well as degenerative effects incurred during healthy aging (Arani *et al.*, 2015; Delgorio *et al.*, 2021; Hiscox *et al.*, 2021; Sack *et al.*, 2011; Takamura *et al.*, 2020). More recently, the emergence of viscoelastic structure-function relationships suggest that indices of brain mechanics are closely related to cognition and behavior with associations observed between MRE measurements and memory performance (Daugherty *et al.*, 2020; Hiscox, Johnson, McGarry, Schwarb*, et al.*, 2020; Schwarb *et al.*, 2017; Schwarb *et al.*, 2016), fluid intelligence (Johnson, Schwarb*, et al.*, 2018), rule learning (Schwarb *et al.*, 2019), risk-taking behaviors (McIlvain *et al.*, 2020), and variations in body-mass index (Hetzer *et al.*, 2020).

As tissue viscoelasticity cannot be measured directly *in vivo*, an MRE scan involves observing the propagation of mechanical vibrations through tissue and follows a three-step process: generating shear waves in the brain, imaging the resulting tissue displacements with a

phase-contrast MRI pulse sequence, and processing these displacements with an inversion algorithm to infer mechanical property maps depicting both elastic and viscous tissue properties (Johnson & Telzer, 2018; Manduca *et al.*, 2001). Methodological advances to both MRE pulse sequences and inversion schemes have resulted in the ability to generate regional property measures, with previous studies highlighting that MRE can reliably quantify the mechanical properties of lobar regions (Murphy *et al.*, 2013), white matter tracts (Johnson *et al.*, 2013), subcortical grey matter structures (Gerischer *et al.*, 2018; Johnson *et al.*, 2016) and, more recently, the hippocampal subfields (Delgorio *et al.*, 2021), all of which have improved the ability to reliably characterize brain health and disease.

While several MRE studies have begun to report results derived from specific regions of the cortex (Hiscox, Johnson, McGarry, Marshall*, et al.*, 2020; Johnson, Schwarb*, et al.*, 2018; McIlvain *et al.*, 2020; Schwarb *et al.*, 2019) there have been no studies which have systematically evaluated the accuracy of performing cortical MRE, despite its predominant role in cognition and high incidence of pathology in neurological disorders. With an overall average thickness of approximately 2.5 mm (Fischl *et al.*, 2000), cortical tissue consists of a highly folded sheet of neurons which possess an unusually complex geometry with the presence of the folds and creases of the gyri and sulci. These more unusual characteristics present additional challenges in obtaining accurate measurements, and factors such as the imaging spatial resolution and adopted inversion algorithm are expected to be particularly important in their recovery. Moreover, it would be reasonable to assume that these challenges may predominately impact cortical measurements in the elderly and patients with neurodegenerative disorders involving cortical tissue loss and a concomitant increase in cerebrospinal fluid (CSF).

Therefore, the purpose of this study was to assess the accuracy of cortical MRE through a series of realistic, whole-brain simulation experiments. Assessment of the performance of cortical MRE has not been demonstrated rigorously and understanding the impact of different imaging and inversion strategies will both inform best practices and future research directions. We used a finite element model of the brain with realistic material properties of the cortex to generate simulated displacement data akin to information captured during an *in vivo* MRE experiment. We then designed three experiments to investigate how accurately cortical regions of interest (ROIs) were recovered by a nonlinear inversion (NLI) MRE algorithm (McGarry *et al.*, 2012; Van Houten *et al.*, 1999), which is a common inversion pipeline used in clinical brain MRE studies. **Experiment 1** investigated the performance of cortical MRE using displacement data acquired at a 1.25 mm isotropic resolution, and compared results with downsampled 2.0 mm data, to determine whether smaller voxel sizes are needed to accurately reconstruct small cortical areas. **Experiment 2** investigated whether incorporating *a priori* anatomical information within NLI, i.e. through soft prior regularization (McGarry *et al.*, 2013), significantly improved the accuracy of the reconstructed property maps in the complex cortical geometries. Finally, **Experiment 3** examined the performance of cortical MRE in a separate simulation model built from the MRI data of an older participant with mild cognitive impairment (MCI), who displayed greater gyral atrophy and CSF spaces on structural MRI images. The purpose of this final experiment was to determine whether cortical thinning would impact the accuracy of the reconstructed mechanical property outcomes with implications for conducting cortical MRE in patients with more severe neurodegeneration.

Methods

Mechanical properties of the cerebrum and cortical regions of interest (ROIs) were obtained from

in vivo MRE examinations of 20 cognitively healthy older adult participants (mean age: 69±5.9

years) to provide physiologically realistic ground truth mechanical properties for simulation

experiments. The imaging and inversion protocols to obtain these data are described in the

following sections. For the simulation experiments, a nearly incompressible viscoelastic finite-

element (FE) model was built from *in vivo* datasets from representative cases of one of the healthy

older adults initially examined (65 years/female) (Experiments 1 and 2) as well as a participant

with a diagnosis of mild cognitive impairment (MCI) and who displayed significant signs of

cerebral atrophy (75 years/female) (Experiment 3). The study was approved by the Institutional

Review Board of the University of Delaware and all participants provided written informed

consent prior to participation. The research was conducted in accordance with the principles

embodied in the Declaration of Helsinki and in accordance with local statutory requirements.

2.1 Imaging protocol

Imaging data were collected on a Siemens 3T Prisma MRI scanner with a 64-channel head coil

(Siemens Healthineers; Erlangen, Germany). Tissue displacements for MRE were generated at 50

Hz (314.16 rad/sec) by the pneumatic Resoundant actuator and head pillow device (Resoundant;

Rochester, MN, USA). A 3D multiband, multishot spiral MRE imaging sequence was used to

capture displacement data at an isotropic 1.25 mm resolution. Imaging parameters included:

repetition time (TR)/echo time (TE) = 3360/70 ms, 240 x 240 mm^2 field-of-view (FOV); 192x192

matrix; 8 in-plane constant-density spiral shots (Glover, 1999); 96 axial 1.25 mm thick slices (24

volumes of 4 simultaneously excited slices each); undersampling both in-plane (4 k_{xy}-shots

acquired, $R_{xy} = 2$) and through-plane (2 k_z-planes acquired, $R_z = 2$), with an encoding efficiency of 1.233 µm/rad. We have recently used this sequence to generate high-quality displacement data at a 1.25 mm resolution in older adults (Delgorio *et al.*, 2021). The T1-weighted MPRAGE (magnetization-prepared rapidly acquired gradient echo) scan was acquired at a 0.9 mm isotropic resolution (TR/TI/TE = 1900/900/2.32 ms).

2.2 MRE reconstruction

Nonlinear inversion (NLI) is an iterative technique that minimizes an objective function which compares a heterogeneous nearly incompressible viscoelastic computational model with the measured displacement data of tissue under external harmonic excitation (McGarry *et al.*, 2012; Van Houten *et al.*, 1999; Van Houten *et al.*, 2000). NLI inversions reported here applied the same parameters commonly used for *in vivo* brain imaging (Delgorio *et al.*, 2021; Hiscox, Johnson, McGarry, Marshall*, et al.*, 2020; McIlvain *et al.*, 2020; Schwarb *et al.*, 2019). The assumption of near incompressibility is implemented through a mixed u-p formulation with the bulk modulus fixed at $K = 1000$ kPa to provide a Poisson ratio of 0.49 (Zienkiewicz *et al.*, 1977). The material property mesh resolution was equal to the measurement resolution (1.25 mm) and smoothing was applied between global iterations. NLI parameter updates involved two conjugate gradient iterations with two-line search iterations per subzone, 25 mm subzones with 15% overlap, and 100 global iterations were allowed for convergence. Inversions were executed on a quadratic 27-node hexahedral finite element mesh which was generated from a 3D mask created from the acquired displacement data with nodal spacing equal to the measurement resolution. The unknown G' and G" values were supported on an 8-node hexahedral mesh at the same resolution (McGarry *et al.*, 2012). After convergence, G' and G" values were converted to quantitative maps of shear stiffness,

$\mu = 2\ |G^*|^2 / (G' + |G^*|)$, and damping ratio, $\xi = G''/2G'$. The shear stiffness describes the resistance of the material to shear deformation, which is a function of frequency. The specific stiffness values provided throughout this study determine the propagation speed of a shear wave at the frequency of measurement, $v_s(\omega) = \sqrt{\frac{\mu}{\rho}}$. The damping ratio is a dimensionless quantity that indicates the level of attenuation in viscoelastic materials (for $\xi > 1$, motion decays rapidly without oscillation).

2.3 Cortical regions of interest

Masks for cortical regions of interest (ROIs) were obtained via automatic segmentation of the subject-specific T1-weighted images using Freesurfer v.6.0 (Fischl *et al.*, 2002) with anatomical boundaries based on the Desikan-Killiany cortical parcellation atlas (Desikan *et al.*, 2006). Six cortical regions of interest (ROIs) were investigated based on their vulnerability to cortical atrophy due to aging, mild cognitive impairment (MCI), or Alzheimer's disease (AD). The ROIs included the middle temporal gyrus (MTG), parahippocampal gyrus (PHC), posterior cingulate cortex (PCC), precentral gyrus (PCG), precuneus cortex (PNS), and superior temporal gyrus (STG) (Du *et al.*, 2007; Hiscox, Johnson, McGarry, Marshall, *et al.*, 2020; Krumm *et al.*, 2016; Salat *et al.*, 2004). These selections were also based on neuroanatomical location for investigation into the variability of results due to ROIs positioned either on the cortical surface, next to the interhemispheric (longitudinal) fissure, or within the medial temporal lobe. Advanced normalization tools (ANTS) (Avants *et al.*, 2011) was used to co-register the cortical masks from MPRAGE space to MRE native space and were thresholded at 50% to create binary masks.

2.4 Measured realistic material properties

Results from the 20 participants are provided in Table 1. All measurements were computed from the whole brain property maps and without erosion of voxels from the cortical masks. Most cortical ROIs are softer than the cerebrum, which is consistent with both in vivo and ex vivo reports that the cortex is softer than the global cerebrum and white matter (Braun *et al.*, 2014; Budday *et al.*, 2015; Hiscox, McGarry*, et al.*, 2020). From these measurements, we calculated the mean ± two standard deviations for each cortical ROI for both μ and ξ and used the randomize function within MATLAB to obtain 20 random measures from a uniform distribution within this range.

Table 1. Measurements obtained from in vivo MRE data of 20 healthy older adult participants that were assigned to the cerebrum (background) and cortical ROIs for simulation of displacement fields.

Region	μ (M±SD)	μ (Range)	ξ (M±SD)	ξ (Range)
Cerebrum (CE)	2.57±0.16	2.26-2.88	0.256±0.009	0.238-0.273
Middletemporal gyrus (MTG)	2.31±0.23	1.85-2.78	0.323±0.031	0.261-0.384
Parahippocampus cortex (PHC)	2.70±0.27	2.17-3.24	0.156±0.021	0.113-0.198
Posterior cingulate cortex (PCC)	2.61±0.29	2.02-3.19	0.143±0.058	0.027-0.260
Precentral gyrus (PCG)	2.09±0.26	1.58-2.60	0.292±0.029	0.233-0.351
Precuneus (PNS)	2.50±0.18	2.14-2.86	0.168±0.024	0.121-0.215
Superiortemporal gyrus (STG)	2.26±0.22	1.82-2.71	0.341±0.031	0.279-0.403

M = mean; SD = standard deviation.

2.5 Simulation experiments

To produce realistic wavefields, whole-brain FE models were built at the MRE resolution (1.25mm) and driving boundary conditions were taken from MRE displacement data on the brain surface. The bottom surface of the fixed boundary conditions remained stress free to avoid

unrealistic dilatational stresses from fully constraining the boundaries with noisy experimental data. Anatomical regions were prescribed from the subject-specific high-resolution T1-weighted imaging data, after registration with ANTS to MRE native space (with nearest neighbor interpolation). The material property mesh resolution (McGarry *et al.*, 2012) was set to half of the displacement mesh resolution to allow the highest property resolution possible to be supported. Random measurements within the range of values provided in Table 1 were prescribed as the "ground truth" for the cerebrum and each cortical ROI, with identical measurements prescribed in all models. As different sets of displacement boundary conditions have a limited effect on the accuracy of the inversions of simulated data, we limited the study to one representative set from each group due to the large number of simulations required in these experiments and heavy computational burden of 3D finite element solutions at high resolution. More details on the FEM simulation platform can be found in McGarry *et al.* (2021).

Fluid-solid interaction was not available in our simulation platform; therefore, fluid (CSF) spaces were modelled as a very soft solid to approximate the *in vivo* conditions. CSF maps were obtained via the segment tool in SPM (Statistical Parametric Mapping software, http://www.fil.ion.ucl.ac.uk/spm/) and co-registered to MRE space using the same ANTS transform (Section 2.3) and thresholded at 50%. A relatively low real shear modulus (0.3 kPa) and high loss modulus (0.3 kPa) was prescribed to fluid spaces, providing 8 nodes per shear wavelength to avoid excessive discretization errors (McGarry *et al.*, 2012). Although this only provides an approximation of fluid behavior, the simulated low shear modulus and high damping ratio has been used to represent CSF in models of brain biomechanics (Giudice *et al.*, 2021).

The simulated datasets were then interpolated to the measurement resolution to simulate MRI measurement, and Gaussian noise (standard deviation equal to 2% of the mean absolute

displacement values) was added to the synthetic data to simulate measurement uncertainty. Altogether, twenty separate simulations were generated with varying background (cerebrum) and cortical measurements. This simulated output from the FE model was then used as input for NLI to investigate performance in an idealized situation where "true" properties are known. NLI inversion parameters were the same as those applied in clinical brain studies, previously described in Section 2.2. A summary of the simulation procedure is provided in **Figure 1.**
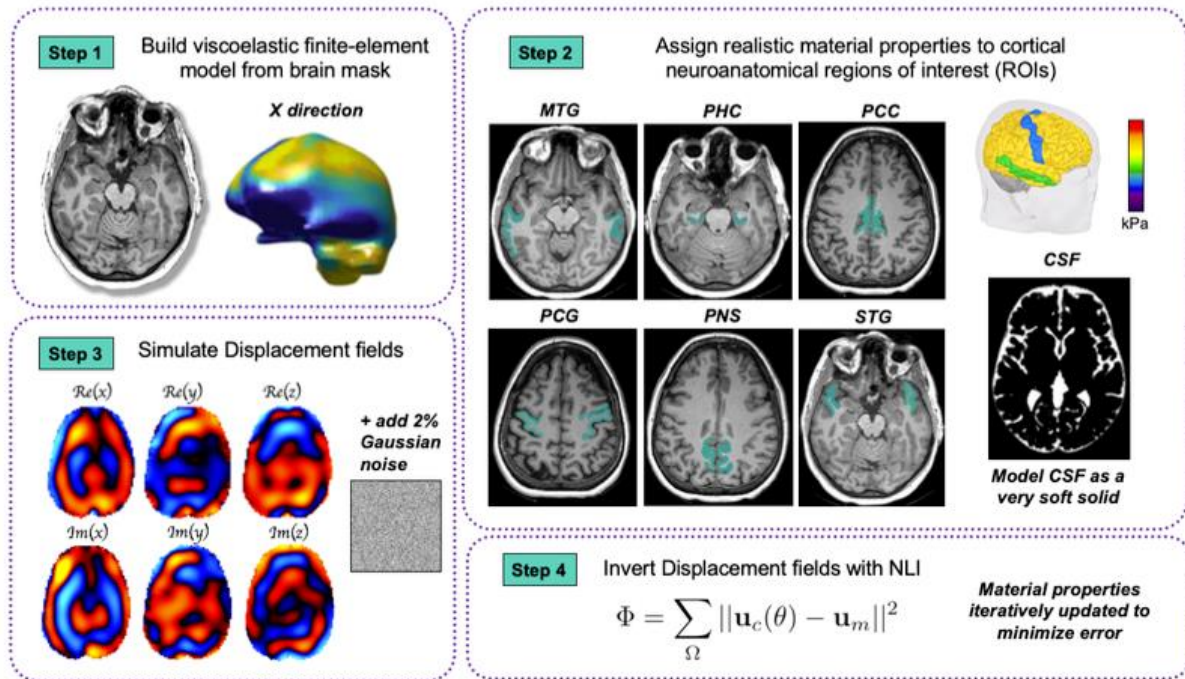

Figure 1. Summary of MRE simulation process. In Step 1, a nearly incompressible viscoelastic finite-element model is generated from the brain mask driven by realistic wavefield boundary conditions and mechanical properties from MRE data of a single subject. In Step 2, realistic material properties are assigned to each cortical ROI, such as the precentral gyrus (blue) and the middletemporal gyrus (green), and CSF is modelled as a very soft material. The background (i.e., other regions of the brain that are not one of the 6 cortical ROIs) are held constant (yellow) but vary between each simulation. In Step 3, simulated displacement fields in x, y, and z, are generated from the properties assigned in Step 2. Random Gaussian noise is applied to simulate measurement uncertainty, providing a realistic OSS-SNR comparable to that observed in *in vivo* MRE. The final step involves the reconstruction of material properties from the simulated displacement fields using the standardized parameters from NLI, unless otherwise stated.

2.6 Summary of experiments

Experiment 1: Effect of displacement data spatial resolution

In this experiment, we assessed the impact of spatial resolution (smaller voxel sizes) on the accuracy of the recovered properties. In addition to the creation of simulated displacement fields based on 1.25 mm isotropic MRE data (see Section 2.5), we also downsampled the same simulated data to a 2.0 mm isotropic resolution by truncation in frequency space and compared the accuracy of the two measurements to the prescribed truth. Although in practice higher resolution data often comes with an SNR penalty, the same amount of Gaussian noise (standard deviation equal to 2% of the mean absolute displacement values) was applied to both 1.25 mm and the downsampled 2.0 mm data to isolate the effect of higher resolution input data from the effects of noise — i.e., input data regardless of resolution is assumed to be high quality with sufficient SNR. The resulting octahedral shear strain signal-to-noise ratios (OSS-SNRs) for simulated 1.25 mm datasets was 4.67 ± 0.12 and for the 2.0 mm datasets was 8.34 ± 0.22. These OSS-SNR values are above the minimum of 3.0 considered necessary for stable inversion (Hannum *et al.*, 2021; McGarry *et al.*, 2013). All NLI parameters were set to the default settings, except for alterations to the spatial filter width (SFW) which is dependent on the imaging resolution. SFW in NLI controls how much smoothing is applied between subzones during a global iteration to regularize the solution. In most published literature, SFW has been set to 1.5 mm to maintain consistency between studies, regardless of the nominal imaging spatial resolution. However, as higher resolution displacement data becomes available, decreasing SFW is an attractive option as it will reduce smoothing and regularization of the solution to sharpen MRE property maps (Delgorio *et al.*, 2021), and the higher density of measured data points will help to maintain the stability usually provided by larger SFW (McGarry *et al.*, 2017). For this work, we maintained the SFW at 1.5 mm for 2.0 mm MRE data

and reduced the SFW to 0.9 mm for the higher resolution 1.25 mm displacement data. We hypothesized that higher spatial resolutions would lead to more accurate mechanical property reconstruction with recovered measures closer to those prescribed in simulation. Soft prior regularization (SPR) was not applied in this first experiment.

Experiment 2: Impact of soft prior regularization (SPR)

SPR is a technique that incorporates *a priori* spatial information from an anatomical MRI scan within the inversion to penalize variation in properties within prescribed regions. SPR is often used in conjunction with NLI and has previously been shown to improve measurement accuracy in simulations (McGarry *et al.*, 2013) and repeatability in *in vivo* studies of smaller structures (Delgorio *et al.*, 2021; Johnson *et al.*, 2016). SPR is controlled by a scalar weighting, α, which balances a regularization term in the NLI objective function that penalizes intra-region heterogeneity to prefer homogeneous property solutions against reduction in the displacement error and potentially reduces influence from neighboring tissues or CSF. In this experiment, the performance of three different SPR α weightings ($\alpha = 10^{-10}$, 10^{-11}, and 10^{-12}) were investigated to determine the optimal α weighting for the cortex, which are all within the range used in previous literature (Hiscox, Johnson, McGarry, Marshall*, et al.*, 2020; Johnson, Schwarb*, et al.*, 2018). When SPR is active, no smoothing across regional boundaries was allowed during the spatial filtering process to potentially further improve regional property estimates.

Experiment 3: Effect of cortical atrophy

Aging and neurodegenerative disorders are well-documented causes of cortical thinning (Kemper, 1994; Salat *et al.*, 2004); as a result, accurate recovery of mechanical properties with MRE may

be particularly challenging in smaller tissues due to gyral atrophy and fluid (CSF) spaces. We built a further separate FE model based on MRE and anatomical information from a participant with MCI that displayed cortical atrophy relative to the healthy adult participant previously described; this model will be subsequently referred to as the *atrophy* model throughout the rest of the paper. Prescribed mechanical properties for simulation of displacement fields were identical to those prescribed in the healthy model, as shown in Table 1, to ensure that only the variation in geometry and boundary conditions were examined. Simulated displacement fields were then analyzed with the optimized NLI protocol (based on the outcomes from Experiments 1 and 2) and accuracy in recovered properties was compared with results from the healthy brain model.

2.7 Statistical analyses

To determine the accuracy of cortical MRE, analyses included assessing the mean absolute error (MAE) between the true prescribed simulated measurements versus the NLI reconstructed inverted measurements, MAE = |inversion-truth|. Paired samples t-tests (two-tailed) were used to determine if MAE differed according to the spatial resolution (Experiment 1), whereas one-way ANOVAs with Bonferroni corrected post-hoc comparisons were used to investigate the impact of SPR α weighting on MAE scores (Experiment 2). Independent samples *t*-tests were also used to assess mean differences between the healthy vs atrophy model using the optimized protocol (Experiment 3). Statistically significant effects were determined at $p < 0.05$. Linear regression was also applied to examine the slope (*y*) from each method, comparing *y* with the slope from the true results (IV = outcome; DV = simulated ground truth) holding the intercept at 0. All Statistical analyses were conducted using Stata, version 17.0 (Statacorp, College Station, TX).

3. Results

Experiment 1: Effect of displacement data spatial resolution

In the first experiment, we examined the effect of the MRE displacement spatial resolution on the accuracy of the recovered properties from NLI by comparing MAE scores between 1.25 mm and 2.0 mm motion data (**Table 2**). For reference, all MRE measurements (quantitative values of μ and ξ) are provided in the Supplementary Material (Table S1).

Overall, imaging spatial resolution had a moderate impact on the accuracy of the recovered properties. A higher spatial resolution of 1.25 mm reduced the average μ MAE by nearly 30% when compared with 2.0 mm MRE data (μ: 0.18 kPa *vs.* 0.23 kPa, respectively). This corresponds to an average error of 9.4% for 2.0 mm, and 7.2% for 1.25 mm data. Notably, PHC had the largest MAE for 2.0 mm simulations (17.3%) which may be related to the smaller number of voxels encompassed within the mask ($n = 615$); error was reduced to 13.2% at a 1.25 mm voxel size (number of voxels, $n = 1843$).

Similarly, MAE for ξ was reduced by 21% with higher spatial resolution simulations compared to 2.0 mm data (ξ: 0.043 v. 0.055, respectively). This corresponds to an average error of 28.7% and 22.9% for 2.0 mm and 1.25 mm data, respectively. Statistical tests showed how higher resolution simulations significantly reduced MAE for all cortical ROIs for both properties ($p < 0.001$), except for PCG, ξ ($p = 0.24$).

Figures 2 illustrates the comparison between the ground truth and example MRE maps from both imaging resolutions, for μ and ξ, respectively. **Figure 3** shows scatter plots illustrating the relationship between the simulated (truth) and recovered (inverted) properties, according to MRE imaging spatial resolution, for μ and ξ, respectively. Notably, the slope of the recovered vs ground truth stiffness of all structures were positive, but less than 1 due to incomplete contrast recovery

in the regularized inversion process. A comparison between the ground truth and example MRE

maps from both imaging resolutions are also presented.

Table 2. Mean absolute error (MAE) of recovered cortical properties depending on the spatial resolution of simulated MRE displacement data.

|	2.0 mm			1.25 mm		
μ	MAE	% Error	No. of voxels	MAE	% Error	No. of voxels
MTG	0.12±0.09	5.3%	2942	0.10±0.07	4.1%	9095
PHC	0.46±0.27	17.3%	615	0.35±0.23	13.2%	1843
PCC	0.22±0.24	8.6%	945	0.19±0.21	7.7%	2887
PCG	0.16±0.14	7.8%	3963	0.13±0.11	6.2%	12462
PNS	0.26±0.13	10.2%	2833	0.19±0.10	7.6%	8899
STG	0.16±0.10	6.9%	3501	0.10±0.08	4.5%	10861
Average	0.23±0.16	9.4%	-	0.18±0.13	7.2%	-
ξ						
MTG	.032±.024	9.9%	-	.021±.015	6.4%	-
PHC	.073±.022	47.2%	-	.055±.018	35.2%	-
PCC	.077±.037	56.8%	-	.067±.033	49.3%	-
PCG	.044±.027	14.3%	-	.041±.023	13.4%	-
PNS	.045±.017	27.4%	-	.036±.014	21.6%	-
STG	.058±.043	16.6%	-	.041±.033	11.8%	-
Average	.055±.028	28.7%	-	.043±.023	22.9%	-
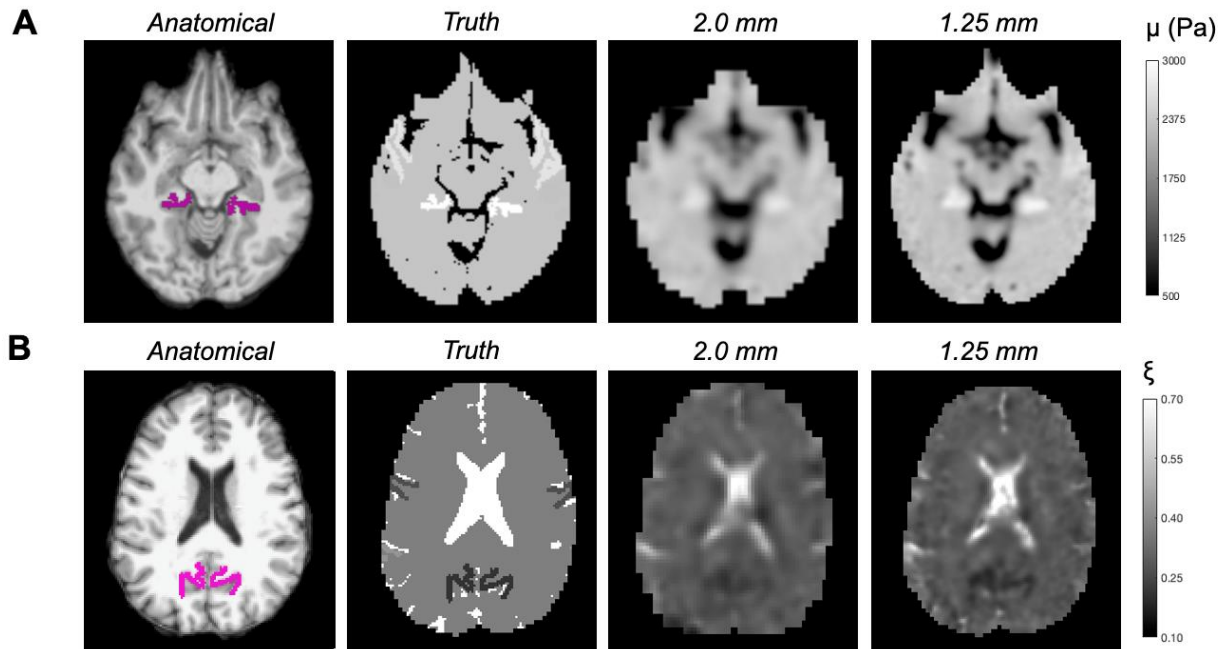
Figure 2: Illustration of MRE maps due to the imaging spatial resolution for (a) shear stiffness, μ, and (b) damping ratio, ξ. Reconstructed images show the benefits of higher spatial resolutions, with evidently sharper property maps, that more closely resemble the simulated ground truth. In the first row, the parahippocampal gyrus (PHC) is outlined on the anatomical T1-weighted image; stiffness of the PHC obtained at a 1.25 mm resolution more closely matches the prescribed material properties, i.e., "truth", when compared with 2.0 mm data. In the second row, the precuneus (PNS) is outlined on the anatomical T1-weighted image. The low damping ratio of the PNS relative to the background (cerebrum) is more clearly displayed at a 1.25 mm resolution. Note that ξ is a dimensionless quantity.
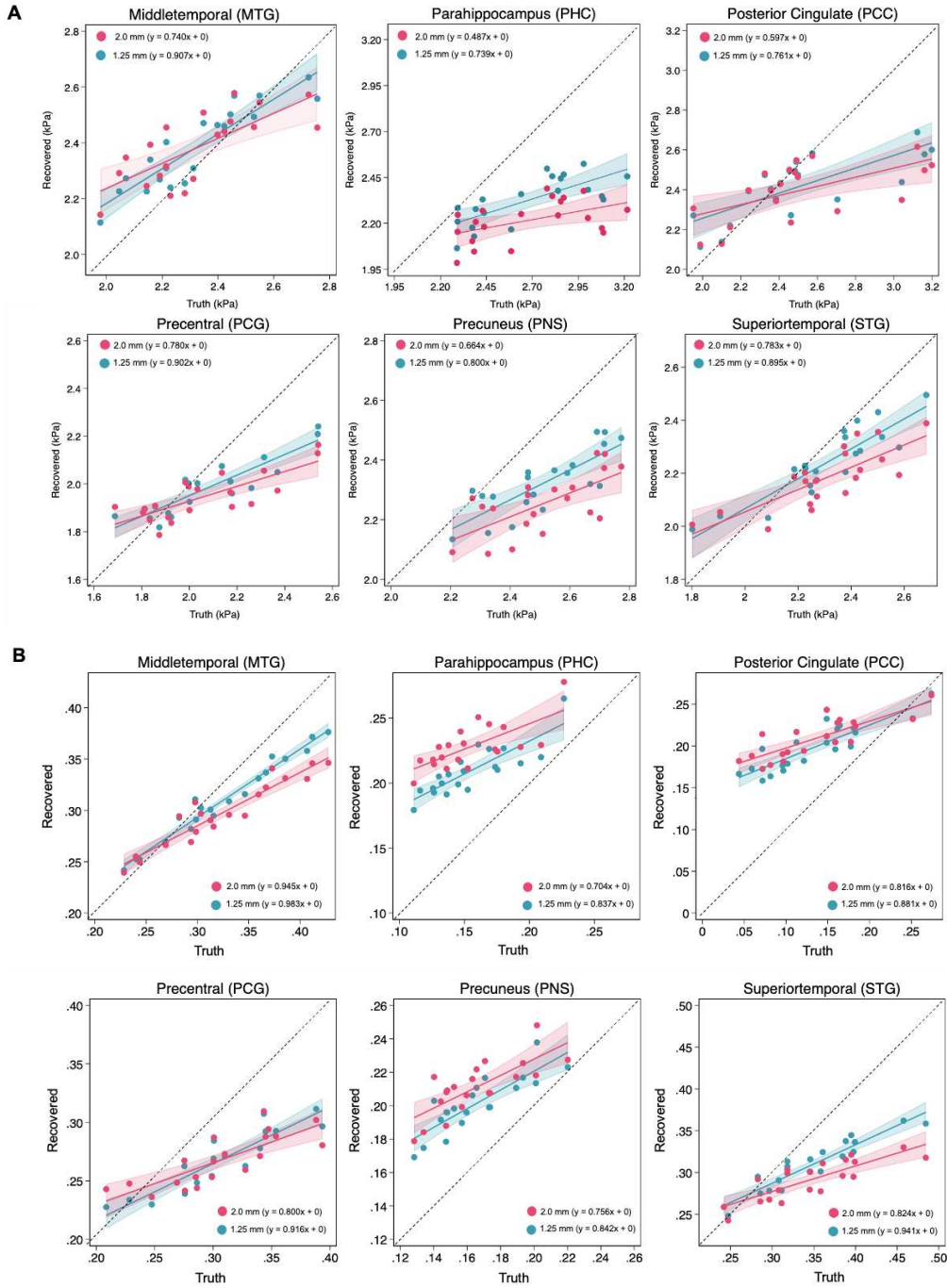
Figure 3: Simulated (truth) versus reconstructed (inverted) measurements for (a) MRE shear stiffness, μ and (b) damping ratio, ξ. For all six cortical ROIs, increasing the spatial resolution from 2.0 mm to 1.25 mm reduced MAE scores, with measurements being closer to the truth (black dotted line).

Experiment 2: Impact of soft prior regularization (SPR)

In the next experiment, we investigated whether incorporating prior spatial information further improved measurement accuracy of 1.25 mm displacement data and compared the effect of three α weightings that have been used in published studies ($\alpha = 10^{-10}$, 10^{-11}, and 10^{-12}).

In general, SPR improved accuracy of both μ and ξ parameters (Table 3; Figure 4). The lowest MAE between the simulated truth and reconstructed inversion measures was observed for SPR $\alpha = 10^{-12}$. On average, MAE for μ significantly decreased from 0.18 kPa (without SPR) to 0.08 kPa with SPR $\alpha = 10^{-12}$ ($p < 0.001$), corresponding to an average error of 7.02% and 3.09% for no SPR and SPR $\alpha = 10^{-12}$, respectively.

MAE for ξ also decreased from 0.043 (without SPR) to 0.021 with SPR $\alpha = 10^{-12}$ ($p < 0.001$), which reduced the average error from 22.9% to 11.2%. Comparable error scores were observed for $\alpha = 10^{-11}$ for both parameters, although slightly higher average MAE values across all ROIs are reported (Table 3). While $\alpha = 10^{-10}$ showed improved scores relative to inversion without SPR (μ: 0.13 kPa; ξ: 0.032), the reduction in error was not statistically significant for either measure (μ: $p = 0.44$; ξ: $p = 0.09$) and MAE for both parameters were significantly larger than those reported for both $\alpha = 10^{-12}$ and $\alpha = 10^{-11}$. An illustration of MRE property maps according to α weighting is provided in Figure 5.

Table 3. Mean absolute error (MAE) of recovered cortical properties dependent on soft prior regularization (SPR) α weighting.

|	SPR α = 10^{-12}		SPR α = 10^{-11}		SPR α = 10^{-10}	
μ	MAE	% Error	MAE	% Error	MAE	% Error
MTG	0.04±0.02	1.61%	0.04±0.03	1.79%	0.06±0.04	2.59%
PHC	0.14±0.10	5.32%	0.13±0.10	4.93%	0.13±0.11	4.80%
PCC	0.15±0.07	5.89%	0.16±0.07	6.23%	0.36±0.25	14.51%
PCG	0.04±0.03	2.16%	0.06±0.03	2.78%	0.11±0.06	5.46%
PNS	0.05±0.03	2.18%	0.06±0.04	2.42%	0.05±0.04	2.18%
STG	0.03±0.03	1.40%	0.04±0.03	1.59%	0.06±0.04	2.43%
Average	0.08±0.05	3.09%	0.08±0.05	3.29%	0.13±0.09	5.33%
ξ						
MTG	.009±.006	2.63%	.009±.006	2.91%	.017±.014	5.33%
PHC	.011±.006	6.85%	.010±.006	6.54%	.011±.006	7.34%
PCC	.041±.021	30.3%	.046±.024	34.03%	.077±.038	56.65%
PCG	.018±.010	5.80%	.020±.012	6.63%	.017±.012	5.39%
PNS	.023±.008	14.07%	.026±.008	15.74%	.032±.010	19.07%
STG	.026±.015	7.45%	.026±.017	7.46%	.039±.023	11.14%
Average	.021±.011	11.18%	.023±.012	12.25%	.032±.017	17.49%
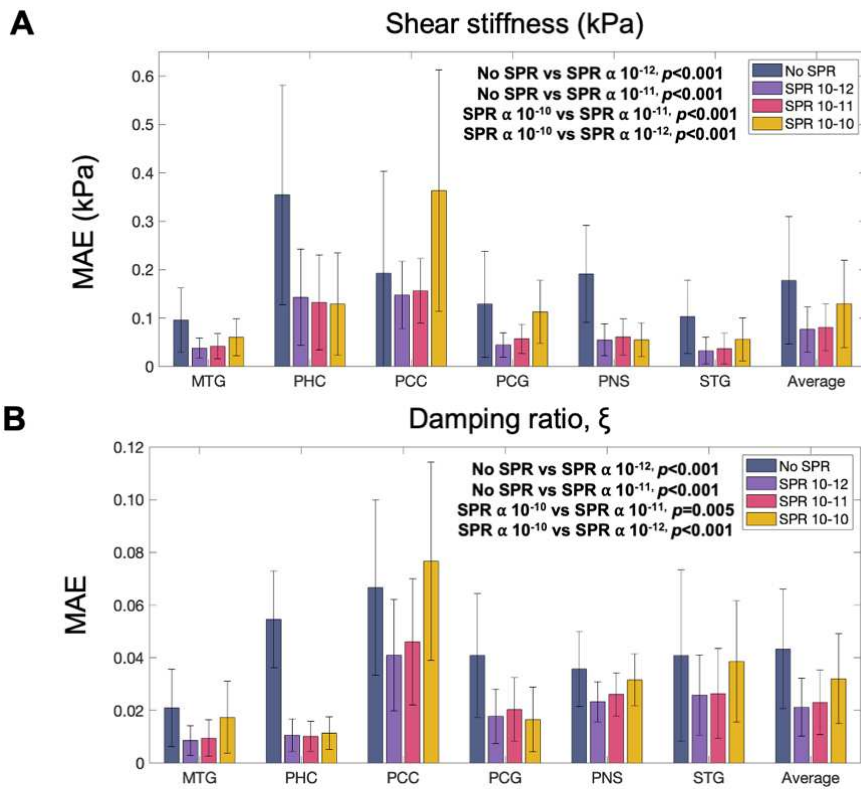
Figure 4. Mean absolute error (MAE) according to SPR α regularization weighting for MRE parameters (a) shear stiffness, μ, and (b) damping ratio, ξ. For both measures, post-hoc comparisons from a one-way ANOVA revealed that MAE results from SPR $\alpha = 10^{-12}$ and $\alpha = 10^{-11}$ were significantly lower compared to when SPR wasn't applied (no SPR). SPR $\alpha = 10^{-12}$ and $\alpha = 10^{-11}$ also yielded significantly lower MAE scores compared to $\alpha = 10^{-10}$.
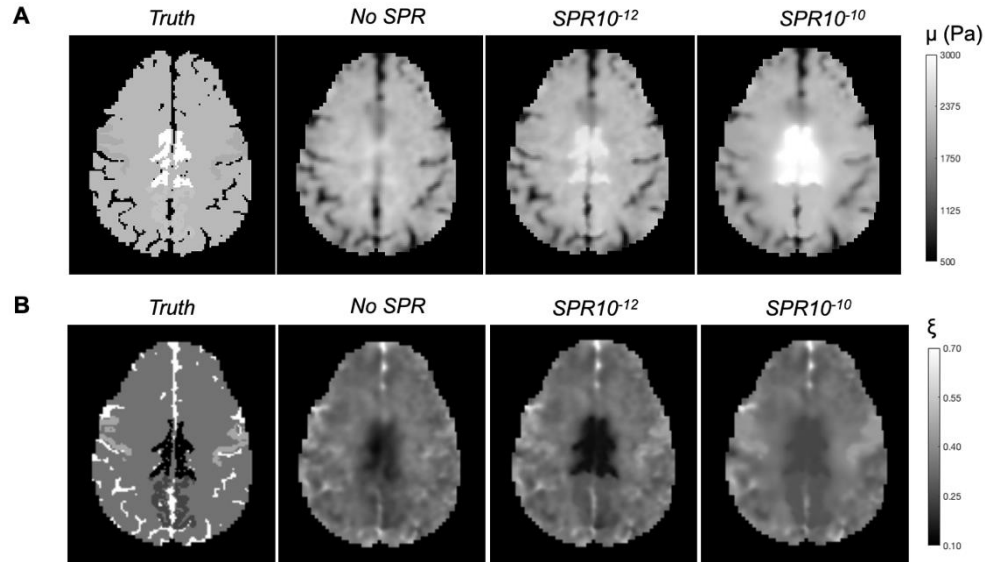
Figure 5. Illustration of MRE maps according to SPR α regularization weighting for MRE parameters (a) shear stiffness, μ, and (b) damping ratio, ξ. The benefits of SPR with a lower regularization weighting ($\alpha = 10^{-12}$) are apparent when considering the reconstruction of the posterior cingulate cortex (PCC); MRE values are similar to the simulated ground truth. Greater measurement error is evidently higher for the PCC with the application of $\alpha = 10^{-10}$; in this case, both stiffness and damping ratio properties are overestimated. Note that ξ is a dimensionless quantity.

Experiment 3: Effect of cortical atrophy

In the final experiment, the accuracy of cortical MRE in an atrophy model was examined using the optimized protocol as revealed through Experiments 1 and 2 (i.e., 1.25 mm displacement data, SPR $\alpha = 10^{-12}$). Cortical thickness estimates from Freesurfer are provided to illustrate how the two models differed (healthy vs. atrophy).

Average cortical thickness was 2.28 mm for the atrophy model, and 2.60 mm for the healthy model (-0.32 mm thinner; 13% thinning in atrophy compared with healthy aging model). Additionally, reduced thickness in the atrophy model was confirmed in all six of the cortical ROIs: MTG: 2.58 mm vs. 3.04 mm (16% thinner); PHC: 2.52 mm vs. 3.08 mm (20% thinner); PCC: 2.31 mm vs. 2.47 mm (7% thinner); PCG: 2.46 mm vs. 2.70 mm (9% thinner); PNS: 2.08 mm vs. 2.54 mm (20% thinner); STG: 2.37 mm vs. 3.04 mm (25% thinner). The structural characteristics of the brain in both models is illustrated in **Figure 6**.
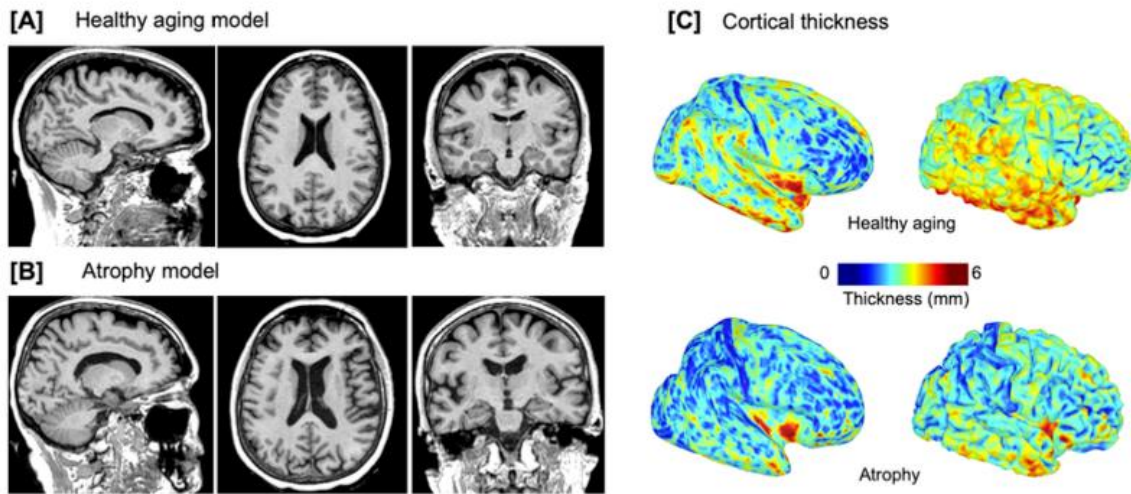
Figure 6. Structural anatomical T1-weighted images demonstrate variation in the levels of cortical thickness which set the boundary conditions for (A) the healthy 65-year-old aging model, and (B) the atrophy model which utilized MRE data from a 75-year-old participant with mild cognitive impairment (MCI); (C) cortical thickness maps from the two participants (scaled from 0-6 mm) clearly demonstrate distinctively different cortical thickness estimates throughout the brain.

A full summary of MAE results from the atrophy model (including statistical tests) are provided in the Supplementary Material (Table S2).

Overall, the average MAE for μ across all ROIs in the atrophy model was 0.09 kPa ± 0.10 kPa, which did not significantly differ from the results obtained from the healthy aging model (0.08 kPa ± 0.07 kPa; $p = 0.17$). Considering individual ROIs, higher error scores were obtained in the atrophy model for PHC ($p = 0.041$), PNS ($p = 0.028$), and STG ($p = 0.004$). Conversely, error for MTG was higher in the healthy model ($p = 0.005$). Surprisingly, results obtained for ξ were slightly more accurate in the atrophy model compared to the healthy model ($p = 0.022$). Example MRE maps from both models are provide in **Figure 7.**
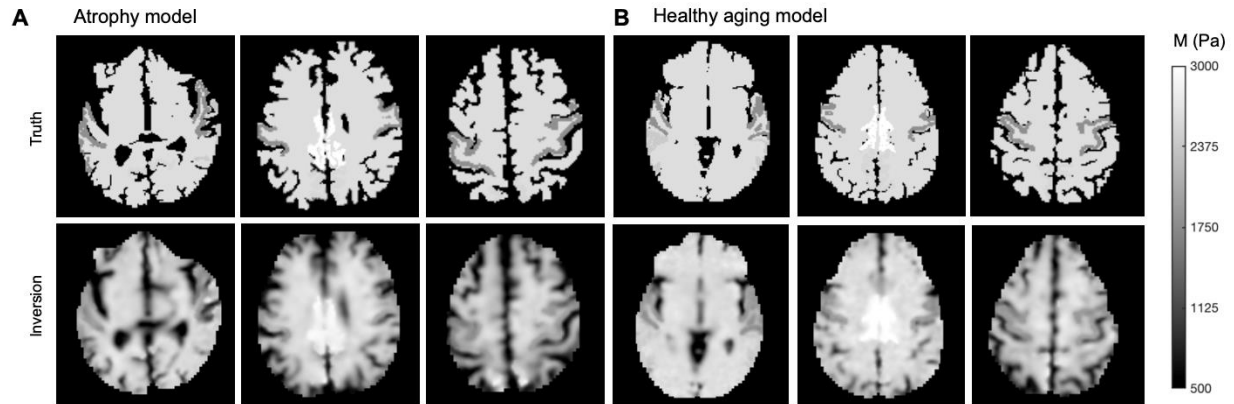
Figure 7. A selection of images from one simulation, with 1.25 mm simulated displacement fields, showing mechanical property recovery based on either (a) the atrophy model, or (b) the healthy aging model. Regardless of the boundary and geometry conditions, identical stiffness measurements are obtained from each model. Note that the increase in fluid spaces in (a) does not appear to distort stiffness values recovered from NLI with SPR.

Scatter plots illustrating the relationship between the simulated (truth) and recovered (inverted) properties, according to each FE model (HC = healthy; MCI = atrophy) are provided in **Figure 8.** As expected, the regression slopes for both models and for all structures are nearly identical. Some issues remain, such as the inability to recover higher stiffness measures, particularly within the PHC, regardless of the thickness of the cortical boundary conditions. Furthermore, there continues to be an overestimation of both MRE measures in midline structures (PCC and PNS), particularly at lower prescribed values.

MRE images of *in vivo* property maps estimated with the optimized NLI protocol from high-resolution displacement data are provided in **Figure 9**. The images presented are from the original MRE experiments that were used to define the boundary conditions for the FE-models used throughout this study, including a healthy older adult and one with MCI.
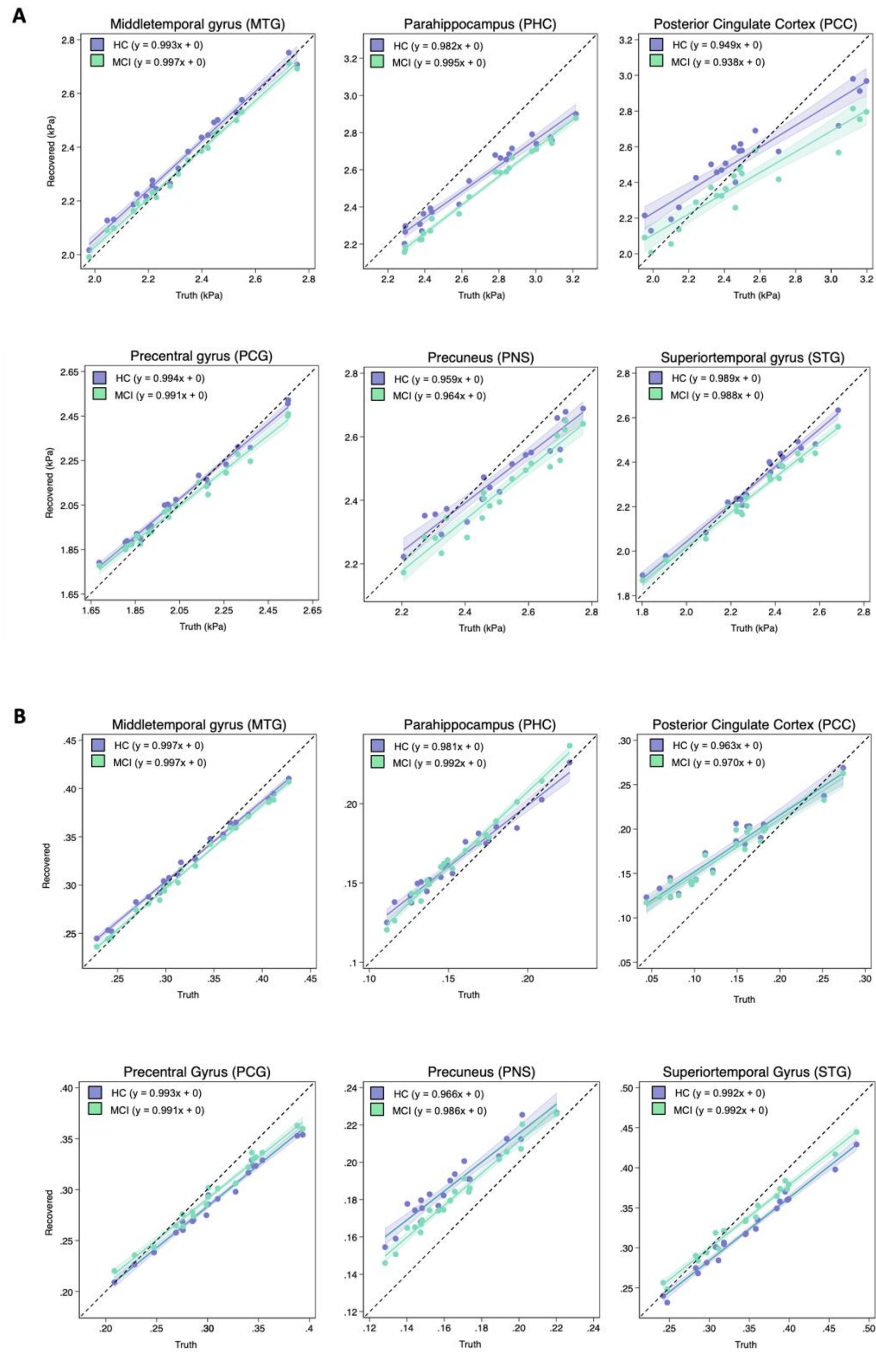
Figure 8. Simulated (truth) versus reconstructed (inverted) measurements for MRE (a) shear stiffness, μ, and (b) damping ratio, ξ. For all six cortical regions of interest (ROIs), similar MAE scores were found for both the healthy aging model (HC) and atrophy model (MCI), with regression slopes both close to 1.
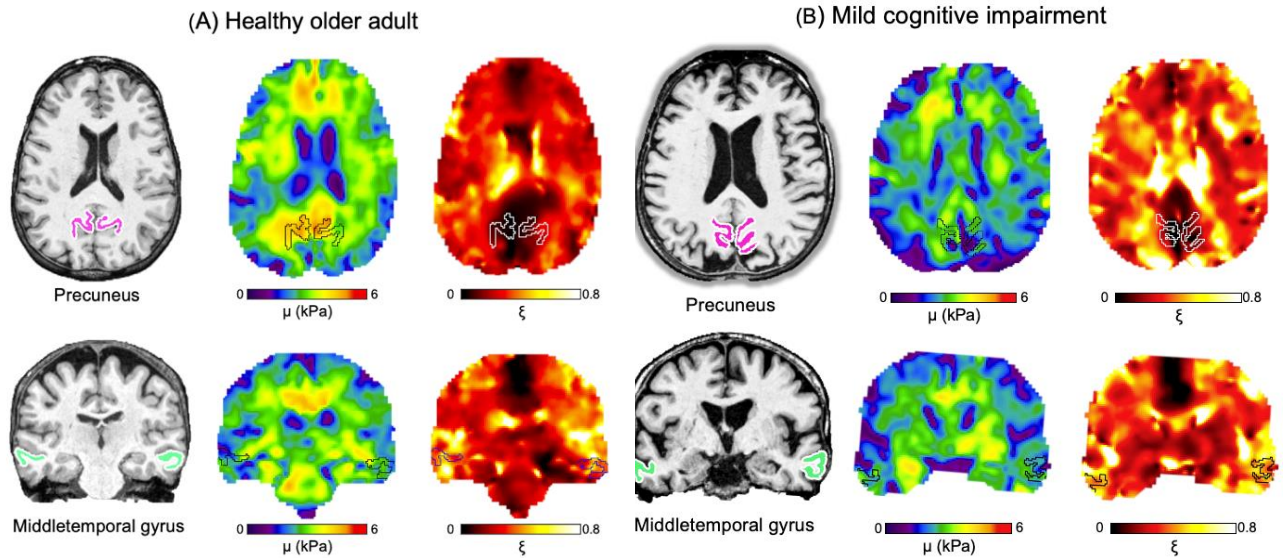
Figure 9. Property maps from *in vivo* MRE estimated from displacement data at 1.25 mm isotropic resolution collected on (A) one healthy older adult (65 years/female) and (B) a participant with a diagnosis of mild cognitive impairment (MCI) (75 years/female). Both stiffness, μ, and damping ratio, ξ, maps are estimated with the optimized NLI parameters from this study. Example cortical regions of the (top) precuneus and (bottom) middletemporal gyrus are outlined.

4. Discussion

This study represents a systematic investigation into the accuracy of using MRE to characterize the mechanical properties of the cerebral cortex *in vivo*. As determining the performance of MRE measurements is not possible *in vivo*, we performed a series of realistic, whole-brain simulation experiments. Here, we provide tentative evidence that MRE measures of the cortex are likely valid for use in both scientific and clinical investigations. We also demonstrate how variation of two methodological considerations on cortical property measures: spatial resolution of the simulated displacement fields and the regularization weighting of *a priori* anatomical information within the inversion, can further enhance the validity of these measures. Finally, we show how the adoption of the optimized protocol provides similar reconstruction accuracy in an atrophy model, in which

the thinning of cortical tissue (i.e., the set geometry and boundary conditions), could reasonably be expected to impact the accuracy of mechanical property recovery.

The principal finding from these experiments is that MRE of thin and irregular structures, such as those observed in the cortex, is feasible with recovered measurements similar to the prescribed ground truth in simulation. Overall, the error margins between the truth and recovered measurements for cortical stiffness are less than 0.08 kPa, which is on the order of 3% total measurement error. Clinical studies have previously reported group differences in global brain stiffness of at least 7% or more (Gerischer *et al.*, 2018; Huston *et al.*, 2016; Murphy *et al.*, 2011; Murphy *et al.*, 2015), with a recent study demonstrating that cortical stiffness can differ in patients with Alzheimer's disease by well over 20% (Hiscox, Johnson, McGarry, Marshall*, et al.*, 2020). As such, the current study reports margins of error lower than published study effects. While *in vivo* MRE experiments contain additional sources of error from known and unknown sources that are not captured through simulation, measuring accuracy *in vivo* is not possible at this time. Thus, the current simulation experiment provides the most robust evidence currently available to illustrate how cortical MRE measures are both valid and useful in scientific investigations.

Our initial analyses from *in vivo* MRE provided realistic material properties of the cortex to generate the simulated displacement fields, and all cortical stiffness values used here were generally lower than the cerebrum that primarily consists of white matter. This is consistent with several *in vivo* human brain MRE studies (Braun *et al.*, 2014; Johnson *et al.*, 2013; Kruse *et al.*, 2008) and is typically consistent with indentation experiments of *ex vivo* animal brains (Budday *et al.*, 2015; Feng *et al.*, 2013; van Dommelen *et al.*, 2010) despite large variations in testing procedures. It is worth noting that only values that the inversion algorithm has previously reported

were included as ground truth, meaning that they likely contain some bias; however, the range of values prescribed were within those reported across the brain MRE literature (Hiscox *et al.*, 2016).

Estimates of cortical μ measurement error are similar to previous simulation (Delgorio *et al.*, 2021; McGarry *et al.*, 2015; McGarry *et al.*, 2021) and phantom studies (Arunachalam *et al.*, 2017; Solamen *et al.*, 2018). In similar simulation experiments, Delgorio *et al.,* report an average error for the hippocampal subfields as -0.24 kPa, with stiffness typically underestimated (Delgorio *et al.*, 2021), whereas McGarry *et al.,* report errors between 0.7-6.9% for a range of brain structures in noise free conditions with no SPR (McGarry *et al.*, 2021). In this study, we show how the stiffness of the cortex is typically underestimated due to incomplete contrast recovery. As a result, our data indicate how the errors in recovered properties are not random; that is, measurement errors do not always appear as noise, but rather can be affected by a uniform under or over-estimation of contrast. This indicates the error has the effect of reducing sensitivity, though not necessarily increasing uncertainty, and future studies may only be disadvantaged from a loss of statistical power and not by random noise or instabilities. While the use of SPR shows improved contrast recovery with appropriately higher stiffness measures (see Supplementary Material Table S1), future studies may benefit from considering the contrast of these structures with the surrounding tissue rather than the absolute recovered property values.

Parameters related to wave attenuation, such as the damping ratio, have been demonstrated to have clinical relevance in a growing number of studies (Chaze *et al.*, 2019; Guo *et al.*, 2013; Lipp *et al.*, 2013; Sandroff *et al.*, 2017; Sinkus *et al.*, 2007). Average cortical ξ measurement error of 0.021 (11%) is proportionally larger to those reported for stiffness but is similar to previous results that show greater difficulty in estimating ξ (Delgorio *et al.*, 2021; McGarry *et al.*, 2021; Solamen *et al.*, 2018). The extra challenge in recovering ξ *in vivo* may be due to the mismatch

between the true mechanisms of energy loss in brain tissue and the simplified attenuation in the viscoelastic model, which may require additional regularization for stability (McGarry *et al.*, 2012). For example, a recent study of the small hippocampal subfields reports how a larger spatial filter width, even greater than the nominal imaging resolution, was needed to balance measurement accuracy, repeatability, and sensitivity (Delgorio *et al.*, 2021). However, our simulated results also demonstrate greater errors in ξ which suggests numerical factors are also relevant. Although the absolute sensitivity of the displacements of a viscoelastic model to changes in the storage and loss modulus are identical, the loss modulus in the numerator for ξ is typically much lower than the storage modulus. Therefore, a similar absolute error in loss modulus produces a larger relative error compared to the storage modulus. Additionally, ξ is a ratio of two reconstructed parameters and thus expected errors in ξ are larger (Shackleford *et al.*, 2016). In the current study, we adopted a spatial filter width appropriate for the nominal imaging resolution, though we also examined whether increasing the spatial filter width to 1.5 mm (from 0.9 mm) improved measurement accuracy of ξ as observed for the hippocampal subfields (see Supplementary Material Table S3). We instead found that measurement error in ξ increased, at a cost in resolution, and thus the greater spatial variation and sharper MRE property maps obtained from a lower spatial filter width was beneficial to ξ reconstruction in this application with the thinner, more finely detailed structures. On this note, NLI has the capability to employ other regularization techniques including total variation minimization and Tikhonov regularization, which were not adopted in this study as to date they have not been applied in clinical studies (McGarry *et al.*, 2017).

As shear waves are used to image properties at sub-wavelength scales, there is likely to be a limit to where higher resolution can improve regional property estimates, meaning that higher resolution data will not necessarily impact outcomes. In the current study, we used simulations to

investigate sub-wavelength resolution in a controlled environment where the ground truth is known. Measures from displacement data downsampled to the poorer 2.0 mm resolution exhibited increased error and smaller slopes indicating reduced sensitivity. Based on resolution alone (without SPR), these differences are modest—with average MAE measures increasing for stiffness by 0.05 kPa and damping ratio by 0.012. These findings support the idea that the greater 1.25 mm resolution improved our property measures, with the higher resolution and concurrent increase in measurement density allowing the use of a lower spatial filter to stabilize the inverse problem. The results provided by the lower 2.0 mm resolution, however, suggest that cortical MRE measurements are not precluded at lower resolution, although more participants would be needed to achieve the same statistical power. In other words, our study confirms both the benefits of higher spatial imaging resolution for quantifying cortical viscoelasticity, while at the same time illustrating how studies performed at lower spatial resolutions will still provide reasonable results.

We found that SPR provides a significant improvement in measurement accuracy, with the lowest regularization (SPR $\alpha = 10^{-12}$) providing the overall greatest benefit for this application. Utilizing 1.25 mm motion data, we found that SPR 10^{-12} reduced error in both stiffness and damping ratio by over 50%, with similar SPR advantages having been reported for subcortical grey matter structures (Johnson *et al.*, 2016) and hippocampal subfields (Delgorio *et al.*, 2021). Of note, we found that the application of SPR $\alpha = 10^{-12}$ provided a substantial benefit to the recovery of PHC, ξ, which reduced measurement error from 35% to 7%. Our results suggest that SPR is particularly important for the cortex, as supplying spatial information will preserve the sharp discontinuities that arise from tissue boundaries lying adjacent to fluid filled spaces in which interfaces across tissue boundaries would otherwise become blurred (McGarry *et al.*, 2013). We chose SPR weights within the range used in previous clinical brain MRE studies; if the

regularization term was much lower, the regional heterogeneity will not be penalized, and the extra spatial information will provide no benefit. In contrast, if the SPR penalty term was much higher, the SPR penalty term in the objective function will overpower the term promoting displacement error reduction and iterative property updates will be very small. In the present study, we did not investigate the use of SPR with 2.0 mm motion data, but it is likely that applying SPR to poorer resolution data would provide similar benefits (Johnson *et al.*, 2016). Another group has recently introduced inversion-recovery MRE (IR-MRE) in an attempt to suppress the CSF signal to provide sharper fluid-solid boundaries of surface areas (Lilaj *et al.*, 2021). By suppressing the fluid oscillations through the imaging sequence, the resulting stiffness maps clearly better depict ground-truth anatomy. However, phase discontinuities across the sulci are still visible, and whether higher stiffness quantification provided by IR-MRE translates to improved accuracy compared with traditional MRE will need to be determined.

We purposely chose to investigate a range of brain structures that were located either on the cortical surface, next to the longitudinal fissure, or within the medial temporal lobe, all of which are known to be affected by aging and in neurodegenerative conditions. Midline structures such as the PCC and PNS showed generally greater error than other structures, particularly in the recovery of ξ. Notably, both PNS and PCC were prescribed a low mean damping ratio and both were largely overestimated (Supplementary Material Table S1) even with the inclusion of the optimal SPR weighting. Low values for midlines structures from *in vivo* MRE may be influenced by data-model mismatch in the estimation of the neighboring *falx cerebri.* The *falx cerebri* is a large, crescent-shaped fold of dura mater that lies between the cerebral hemispheres in the longitudinal fissure. In effect it serves as both a strong discontinuity within the tissue mask (assumed to be a continuous solid) that also acts as a mechanical source (Clayton *et al.*, 2012)

which can impact surrounding property estimates. Furthermore, age-related calcification of both the *falx cerebri* and *tentorium cerebellii* can increase the wave reflection from these membranes (Daghighi *et al.*, 2007; McGrath *et al.*, 2016), which may further impact the accuracy of examining midline structures in older age. Work is ongoing to investigate how the *falx cerebri* should be modelled within MRE. Our simulation and MRE FE models support properties as C∞ continuous functions using the FE basis and property values are defined at the FE nodes. While this is useful for arbitrarily shaped structures which are larger than the mesh solution, modelling a thin, stiff, membrane like the *falx cerebri* would require very fine mesh resolution which makes computing a full brain model computationally challenging. As such, we suggest that MRE measurements of cortical regions on the midline can still be useful, but they should be used with caution.

The majority of post-mortem studies report that cortical thinning and gyral atrophy accelerate during the sixth and seventh decades of life (Kemper, 1994); thus, one of the prevailing concerns with cortical MRE is that the small and complex convolutions of cortical tissue may lend itself to atrophy-related error, thus neutralizing its utility in examining the cortex impacted in aging and dementia. Importantly, this work provides evidence for the contrary, highlighting that the average error for both MRE parameters in an atrophy model are nearly identical to those obtained from a healthy model. The average error of 0.09 kPa (4%) for stiffness is minimal and only marginally greater than the reported 0.08 kPa (3%) average error reported in the healthy model. As a result, we can conclude that cortical thinning, on the order of magnitude observed in age-related neurological conditions, has little bearing on the accuracy of the optimized MRE reconstruction. These results are also supportive of several studies which conclude that anatomical volumes do not correlate with MRE measures (Johnson, Schwarb*, et al.*, 2018; Schwarb *et al.*, 2017), and controlling for volume doesn't effect outcomes of statistical tests (Hiscox, Johnson,

McGarry, Marshall, *et al.*, 2020; Hiscox *et al.*, 2018). A wide range of boundary conditions have also been investigated in previous simulations experiments, which have had minimal impacts on outcomes (McGarry *et al.*, 2021; Tan *et al.*, 2017). While we had access to $n = 10$ MCI and approximately $n = 40$ datasets from healthy older adults, initial experiments showed minimal differences in accuracy. Therefore, we selected a representative case that showed significant signs of atrophy for a more detailed examination. Surprisingly, we found that the aging model yielded greater error scores for ξ (11% vs. 9% error). An explanation for this finding is not immediately clear, but given the very small effect, the impact is unlikely to have any significant impact or clinical relevance. Simulation models from participants with more severe cortical degeneration, such as in the case of Alzheimer's disease were not available, and future work should ensure that simulation results remain consistently accurate to those presented here. Nevertheless, previous studies have reported how cortical thinning due to AD is most prominent in the medial temporal cortex, with a mean magnitude of thinning of 0.4 mm (14% thinning in AD compared with controls) (Dickerson *et al.*, 2009). Thus, the thickness differences tested here (range: 0.16 - 0.67 mm, mean: 0.32 mm) provide a reasonably accurate portrayal of AD atrophy. As a result, we conclude that future MRE studies and their discoveries in clinical populations are likely to be directly related to the intrinsic viscoelasticity of tissue as opposed to an unwanted geometric bias.

This study provides evidence for the accuracy of cortical MRE, although there are still unique challenges that have not been fully addressed. For example, simulation studies are unlikely to be truly representative of *in vivo* elastography due to the presence and constant circulation of CSF as well as internal pressure sources and patient motion. To account for these conditions, we approximated CSF and fluid spaces as a solid tissue continuum, though future work is needed to develop simulation platforms that can model fluid-solid interactions to more accurately represent

in vivo tissue behavior. Similarly, a continuous solid material model was employed through NLI even though the cortex has discontinuous boundaries between the sulci and gyri. While we sought to minimize these effects by increasing spatial resolution and using anatomical information to promote homogeneity within cortical regions (and thus separating them from CSF), cortical MRE measures are likely to benefit from inversion techniques that instead include discontinuous material interfaces with fluid components that follow tissue boundaries. Finally, we applied random Gaussian noise to the motion data to generate measurement uncertainty, though noise in brain MRE, data contains non-Gaussian contributions from physiological sources. At higher OSS-SNR levels, such as those used in this study, the impact of these different noise sources appears similar (Hannum *et al.*, 2021; McIlvain *et al.*, 2022), thus Gaussian noise is sufficient for the purposes of this study. Future work examining regional effects of local noise and other artifacts on cortical MRE regions is necessary.

Conclusions

Localizing mechanical property measurements to specific structures has improved the sensitivity of brain MRE to investigate brain regions that are differentially affected in disease. In this work, we examine the role of MRE spatial resolution, and an inversion scheme designed to improve property measures in pre-defined regions in the ability to accurately recover material properties of the cerebral cortex. In a series of realistic, whole-brain simulation experiments, we found that, in general, the accuracy in the recovery of each cortical structure (middletemporal gyrus, parahippocampus, posterior cingulate, precentral gyrus, precuneus, and superiortemporal gyrus) benefit from higher spatial resolution motion data and nonlinear inversion with a low soft prior

regularization weighting. Additionally, we report that cortical thinning (up to a -0.67 mm reduction in thickness, which is a realistic portrayal of AD-related atrophy) causes no loss in reconstruction accuracy. Taken together, this report of an accurate method to measure cerebral cortex viscoelasticity provides a framework for future MRE investigations to examine cortical degeneration and relationships with health and cognitive functioning.

References

Arani, A., Murphy, M. C., Glaser, K. J., Manduca, A., Lake, D. S., Kruse, S. A., . . . Huston, J., 3rd. (2015). Measuring the effects of aging and sex on regional brain stiffness with MR elastography in healthy older adults. *Neuroimage, 111*, 59-64. doi:10.1016/j.neuroimage.2015.02.016

Arunachalam, S. P., Rossman, P. J., Arani, A., Lake, D. S., Glaser, K. J., Trzasko, J. D., . . . Araoz, P. A. (2017). Quantitative 3D magnetic resonance elastography: Comparison with dynamic mechanical analysis. *Magn Reson Med, 77*(3), 1184-1192. doi:10.1002/mrm.26207

Avants, B. B., Tustison, N. J., Song, G., Cook, P. A., Klein, A., & Gee, J. C. (2011). A reproducible evaluation of ANTs similarity metric performance in brain image registration. *Neuroimage, 54*(3), 2033-2044. doi:10.1016/j.neuroimage.2010.09.025

Braun, J., Guo, J., Lützkendorf, R., Stadler, J., Papazoglou, S., Hirsch, S., . . . Bernarding, J. (2014). High-resolution mechanical imaging of the human brain by three-dimensional multifrequency magnetic resonance elastography at 7T. *Neuroimage, 90*, 308-314. doi:10.1016/j.neuroimage.2013.12.032

Budday, S., Nay, R., de Rooij, R., Steinmann, P., Wyrobek, T., Ovaert, T. C., & Kuhl, E. (2015). Mechanical properties of gray and white matter brain tissue by indentation. *J Mech Behav Biomed Mater, 46*, 318-330. doi:10.1016/j.jmbbm.2015.02.024

Chaze, C. A., McIlvain, G., Smith, D. R., Villermaux, G. M., Delgorio, P. L., Wright, H. G., . . . Johnson, C. L. (2019). Altered brain tissue viscoelasticity in pediatric cerebral palsy measured by magnetic resonance elastography. *Neuroimage Clin, 22*, 101750. doi:10.1016/j.nicl.2019.101750

Clayton, E. H., Genin, G. M., & Bayly, P. V. (2012). Transmission, attenuation and reflection of shear waves in the human brain. *Journal of The Royal Society Interface, 9*(76), 2899-2910. doi:10.1098/rsif.2012.0325

Daghighi, M. H., Rezaei, V., Zarrintan, S., & Pourfathi, H. (2007). Intracranial physiological calcifications in adults on computed tomography in Tabriz, Iran. *Folia Morphol (Warsz), 66*(2), 115-119.

Daugherty, A. M., Schwarb, H. D., McGarry, M. D. J., Johnson, C. L., & Cohen, N. J. (2020). Magnetic Resonance Elastography of Human Hippocampal Subfields: CA3-Dentate Gyrus Viscoelasticity Predicts Relational Memory Accuracy. *J Cogn Neurosci, 32*(9), 1704-1713. doi:10.1162/jocn_a_01574

Delgorio, P. L., Hiscox, L. V., Daugherty, A. M., Sanjana, F., Pohlig, R. T., Ellison, J. M., . . . Johnson, C. L. (2021). Effect of Aging on the Viscoelastic Properties of Hippocampal Subfields Assessed with High-Resolution MR Elastography. *Cereb Cortex, 31*(6), 2799-2811. doi:10.1093/cercor/bhaa388

Desikan, R. S., Ségonne, F., Fischl, B., Quinn, B. T., Dickerson, B. C., Blacker, D., . . . Killiany, R. J. (2006). An automated labeling system for subdividing the human cerebral cortex on MRI scans into gyral based regions of interest. *Neuroimage, 31*(3), 968-980. doi:https://doi.org/10.1016/j.neuroimage.2006.01.021

Dickerson, B. C., Bakkour, A., Salat, D. H., Feczko, E., Pacheco, J., Greve, D. N., . . . Buckner, R. L. (2009). The cortical signature of Alzheimer's disease: regionally specific cortical thinning relates to symptom severity in very mild to mild AD dementia and is detectable in asymptomatic amyloid-positive individuals. *Cereb Cortex, 19*(3), 497-510. doi:10.1093/cercor/bhn113

Du, A.-T., Schuff, N., Kramer, J. H., Rosen, H. J., Gorno-Tempini, M. L., Rankin, K., . . . Weiner, M. W. (2007). Different regional patterns of cortical thinning in Alzheimer's disease and frontotemporal dementia. *Brain, 130*(4), 1159-1166. doi:10.1093/brain/awm016

Feng, Y., Clayton, E. H., Chang, Y., Okamoto, R. J., & Bayly, P. V. (2013). Viscoelastic properties of the ferret brain measured in vivo at multiple frequencies by magnetic resonance elastography. *Journal of Biomechanics, 46*(5), 863-870. doi:https://doi.org/10.1016/j.jbiomech.2012.12.024

Fischl, B., & Dale, A. M. (2000). Measuring the thickness of the human cerebral cortex from magnetic resonance images. *Proc Natl Acad Sci U S A, 97*(20), 11050-11055. doi:10.1073/pnas.200033797

Fischl, B., Salat, D. H., Busa, E., Albert, M., Dieterich, M., Haselgrove, C., . . . Dale, A. M. (2002). Whole brain segmentation: automated labeling of neuroanatomical structures in the human brain. *Neuron, 33*(3), 341-355. doi:10.1016/s0896-6273(02)00569-x

Gerischer, L. M., Fehlner, A., Köbe, T., Prehn, K., Antonenko, D., Grittner, U., . . . Flöel, A. (2018). Combining viscoelasticity, diffusivity and volume of the hippocampus for the diagnosis of Alzheimer's disease based on magnetic resonance imaging. *Neuroimage Clin, 18*, 485-493. doi:10.1016/j.nicl.2017.12.023

Giudice, J. S., Alshareef, A., Wu, T., Knutsen, A. K., Hiscox, L. V., Johnson, C. L., & Panzer, M. B. (2021). Calibration of a Heterogeneous Brain Model Using a Subject-Specific Inverse Finite Element Approach. *Frontiers in Bioengineering and Biotechnology, 9*. doi:10.3389/fbioe.2021.664268

Glover, G. H. (1999). Simple analytic spiral K-space algorithm. *Magn Reson Med, 42*(2), 412-415. doi:10.1002/(sici)1522-2594(199908)42:2<412::aid-mrm25>3.0.co;2-u

Guo, J., Bertalan, G., Meierhofer, D., Klein, C., Schreyer, S., Steiner, B., . . . Sack, I. (2019). Brain maturation is associated with increasing tissue stiffness and decreasing tissue fluidity. *Acta Biomaterialia, 99*, 433-442. doi:https://doi.org/10.1016/j.actbio.2019.08.036

Guo, J., Hirsch, S., Fehlner, A., Papazoglou, S., Scheel, M., Braun, J., & Sack, I. (2013). Towards an Elastographic Atlas of Brain Anatomy. *PLOS ONE, 8*(8), e71807. doi:10.1371/journal.pone.0071807

Hannum, A. J., McIlvain, G., Sowinski, D., McGarry, M. D. J., & Johnson, C. L. (2021). Correlated noise in brain magnetic resonance elastography. *Magn Reson Med*. doi:10.1002/mrm.29050

Hetzer, S., Hirsch, S., Braun, J., Sack, I., & Weygandt, M. (2020). Viscoelasticity of striatal brain areas reflects variations in body mass index of lean to overweight male adults. *Brain Imaging and Behavior, 14*(6), 2477-2487. doi:10.1007/s11682-019-00200-w

Hiscox, L. V., Johnson, C. L., Barnhill, E., McGarry, M. D., Huston, J., van Beek, E. J., . . . Roberts, N. (2016). Magnetic resonance elastography (MRE) of the human brain: technique, findings and clinical applications. *Phys Med Biol, 61*(24), R401-r437. doi:10.1088/0031-9155/61/24/r401

Hiscox, L. V., Johnson, C. L., McGarry, M. D. J., Marshall, H., Ritchie, C. W., van Beek, E. J. R., . . . Starr, J. M. (2020). Mechanical property alterations across the cerebral cortex due to Alzheimer's disease. *Brain Communications, 2*(1). doi:10.1093/braincomms/fcz049

Hiscox, L. V., Johnson, C. L., McGarry, M. D. J., Perrins, M., Littlejohn, A., van Beek, E. J. R., . . . Starr, J. M. (2018). High-resolution magnetic resonance elastography reveals differences in subcortical gray matter viscoelasticity between young and healthy older adults. *Neurobiol Aging, 65*, 158-167. doi:10.1016/j.neurobiolaging.2018.01.010

Hiscox, L. V., Johnson, C. L., McGarry, M. D. J., Schwarb, H., van Beek, E. J. R., Roberts, N., & Starr, J. M. (2020). Hippocampal viscoelasticity and episodic memory performance in healthy older adults examined with magnetic resonance elastography. *Brain Imaging and Behavior, 14*(1), 175-185. doi:10.1007/s11682-018-9988-8

Hiscox, L. V., McGarry, M. D. J., Schwarb, H., Van Houten, E. E. W., Pohlig, R. T., Roberts, N., . . . Johnson, C. L. (2020). Standard-space atlas of the viscoelastic properties of the human brain. *Hum Brain Mapp, 41*(18), 5282-5300. doi:10.1002/hbm.25192

Hiscox, L. V., Schwarb, H., McGarry, M. D. J., & Johnson, C. L. (2021). Aging brain mechanics: Progress and promise of magnetic resonance elastography. *Neuroimage, 232*, 117889. doi:10.1016/j.neuroimage.2021.117889

Huston, J., 3rd, Murphy, M. C., Boeve, B. F., Fattahi, N., Arani, A., Glaser, K. J., . . . Ehman, R. L. (2016). Magnetic resonance elastography of frontotemporal dementia. *Journal of magnetic resonance imaging : JMRI, 43*(2), 474-478. doi:10.1002/jmri.24977

Johnson, C. L., McGarry, M. D. J., Gharibans, A. A., Weaver, J. B., Paulsen, K. D., Wang, H., . . . Georgiadis, J. G. (2013). Local mechanical properties of white matter structures in the human brain. *Neuroimage, 79*, 145-152. doi:10.1016/j.neuroimage.2013.04.089

Johnson, C. L., Schwarb, H., Horecka, K. M., McGarry, M. D. J., Hillman, C. H., Kramer, A. F., . . . Barbey, A. K. (2018). Double dissociation of structure-function relationships in memory and fluid intelligence observed with magnetic resonance elastography. *Neuroimage, 171*, 99-106. doi:10.1016/j.neuroimage.2018.01.007

Johnson, C. L., Schwarb, H., M, D. J. M., Anderson, A. T., Huesmann, G. R., Sutton, B. P., & Cohen, N. J. (2016). Viscoelasticity of subcortical gray matter structures. *Hum Brain Mapp, 37*(12), 4221-4233. doi:10.1002/hbm.23314

Johnson, C. L., & Telzer, E. H. (2018). Magnetic resonance elastography for examining developmental changes in the mechanical properties of the brain. *Developmental Cognitive Neuroscience, 33*, 176-181. doi:https://doi.org/10.1016/j.dcn.2017.08.010

Kemper, T. L. (1994). *Neuroanatomical and neuropathological changes during aging and dementia*.

Krumm, S., Kivisaari, S. L., Probst, A., Monsch, A. U., Reinhardt, J., Ulmer, S., . . . Taylor, K. I. (2016). Cortical thinning of parahippocampal subregions in very early Alzheimer's disease. *Neurobiology of Aging, 38*, 188-196. doi:https://doi.org/10.1016/j.neurobiolaging.2015.11.001

Kruse, S. A., Rose, G. H., Glaser, K. J., Manduca, A., Felmlee, J. P., Jack, C. R., & Ehman, R. L. (2008). Magnetic resonance elastography of the brain. *Neuroimage, 39*(1), 231-237. doi:https://doi.org/10.1016/j.neuroimage.2007.08.030

Lilaj, L., Herthum, H., Meyer, T., Shahryari, M., Bertalan, G., Caiazzo, A., . . . Sack, I. (2021). Inversion-recovery MR elastography of the human brain for improved stiffness quantification near fluid-solid boundaries. *Magn Reson Med, 86*(5), 2552-2561. doi:10.1002/mrm.28898

Lipp, A., Trbojevic, R., Paul, F., Fehlner, A., Hirsch, S., Scheel, M., . . . Sack, I. (2013). Cerebral magnetic resonance elastography in supranuclear palsy and idiopathic Parkinson's disease. *NeuroImage: Clinical, 3*, 381-387. doi:https://doi.org/10.1016/j.nicl.2013.09.006

Manduca, A., Oliphant, T. E., Dresner, M. A., Mahowald, J. L., Kruse, S. A., Amromin, E., . . . Ehman, R. L. (2001). Magnetic resonance elastography: non-invasive mapping of tissue elasticity. *Med Image Anal, 5*(4), 237-254. doi:10.1016/s1361-8415(00)00039-6

McGarry, M., Johnson, C. L., Sutton, B. P., Van Houten, E. E., Georgiadis, J. G., Weaver, J. B., & Paulsen, K. D. (2013). Including spatial information in nonlinear inversion MR elastography using soft prior regularization. *IEEE Trans Med Imaging, 32*(10), 1901-1909. doi:10.1109/tmi.2013.2268978

McGarry, M., Weaver, J., Paulsen, K., & Johnson, C. (2017). *Reconstruction of high-resolution MR elastography motion data using nonlinear inversion.* Paper presented at the Charite MR Elastography workshop.

McGarry, M. D., Johnson, C. L., Sutton, B. P., Georgiadis, J. G., Van Houten, E. E., Pattison, A. J., . . . Paulsen, K. D. (2015). Suitability of poroelastic and viscoelastic mechanical models for high and low frequency MR elastography. *Medical physics, 42*(2), 947-957. doi:10.1118/1.4905048

McGarry, M. D. J., Van Houten, E., Guertler, C., Okamoto, R. J., Smith, D. R., Sowinski, D. R., . . . Paulsen, K. D. (2021). A heterogenous, time harmonic, nearly incompressible transverse isotropic finite element brain simulation platform for MR elastography. *Phys Med Biol*. doi:10.1088/1361-6560/ab9a84

McGarry, M. D. J., Van Houten, E. E. W., Johnson, C. L., Georgiadis, J. G., Sutton, B. P., Weaver, J. B., & Paulsen, K. D. (2012). Multiresolution MR elastography using nonlinear inversion. *Medical physics, 39*(10), 6388-6396. doi:10.1118/1.4754649

McGrath, D. M., Ravikumar, N., Wilkinson, I. D., Frangi, A. F., & Taylor, Z. A. (2016). Magnetic resonance elastography of the brain: An in silico study to determine the influence of cranial anatomy. *Magn Reson Med, 76*(2), 645-662. doi:10.1002/mrm.25881

McIlvain, G., Clements, R. G., Magoon, E. M., Spielberg, J. M., Telzer, E. H., & Johnson, C. L. (2020). Viscoelasticity of reward and control systems in adolescent risk taking. *Neuroimage, 215*, 116850. doi:https://doi.org/10.1016/j.neuroimage.2020.116850

McIlvain, G., McGarry, M. D. J., & Johnson, C. L. (2022). Quantitative effects of off-resonance related distortion on brain mechanical property estimation with magnetic resonance elastography. *NMR in Biomedicine, 35*(1), e4616. doi:https://doi.org/10.1002/nbm.4616

Murphy, M. C., Huston, J., 3rd, Jack, C. R., Jr., Glaser, K. J., Manduca, A., Felmlee, J. P., & Ehman, R. L. (2011). Decreased brain stiffness in Alzheimer's disease determined by magnetic resonance elastography. *J Magn Reson Imaging, 34*(3), 494-498. doi:10.1002/jmri.22707

Murphy, M. C., Huston, J., III, Jack, C. R., Jr., Glaser, K. J., Senjem, M. L., Chen, J., . . . Ehman, R. L. (2013). Measuring the Characteristic Topography of Brain Stiffness with Magnetic Resonance Elastography. *PLOS ONE, 8*(12), e81668. doi:10.1371/journal.pone.0081668

Murphy, M. C., Jones, D. T., Jack, C. R., Jr., Glaser, K. J., Senjem, M. L., Manduca, A., . . . Huston, J., 3rd. (2015). Regional brain stiffness changes across the Alzheimer's disease spectrum. *NeuroImage. Clinical, 10*, 283-290. doi:10.1016/j.nicl.2015.12.007

Muthupillai, R., Lomas, D. J., Rossman, P. J., Greenleaf, J. F., Manduca, A., & Ehman, R. L. (1995). Magnetic resonance elastography by direct visualization of propagating acoustic strain waves. *Science, 269*(5232), 1854-1857. doi:10.1126/science.7569924

Sack, I., Jöhrens, K., Würfel, J., & Braun, J. (2013). Structure-sensitive elastography: on the viscoelastic powerlaw behavior of in vivo human tissue in health and disease. *Soft Matter, 9*(24), 5672-5680. doi:10.1039/C3SM50552A

Sack, I., Streitberger, K.-J., Krefting, D., Paul, F., & Braun, J. (2011). The Influence of Physiological Aging and Atrophy on Brain Viscoelastic Properties in Humans. *PLOS ONE, 6*(9), e23451. doi:10.1371/journal.pone.0023451

Salat, D. H., Buckner, R. L., Snyder, A. Z., Greve, D. N., Desikan, R. S. R., Busa, E., . . . Fischl, B. (2004). Thinning of the Cerebral Cortex in Aging. *Cerebral Cortex, 14*(7), 721-730. doi:10.1093/cercor/bhh032

Sandroff, B. M., Johnson, C. L., & Motl, R. W. (2017). Exercise training effects on memory and hippocampal viscoelasticity in multiple sclerosis: a novel application of magnetic resonance elastography. *Neuroradiology, 59*(1), 61-67. doi:10.1007/s00234-016-1767-x

Schwarb, H., Johnson, C. L., Daugherty, A. M., Hillman, C. H., Kramer, A. F., Cohen, N. J., & Barbey, A. K. (2017). Aerobic fitness, hippocampal viscoelasticity, and relational memory performance. *Neuroimage, 153*, 179-188. doi:10.1016/j.neuroimage.2017.03.061

Schwarb, H., Johnson, C. L., Dulas, M. R., McGarry, M. D. J., Holtrop, J. L., Watson, P. D., . . . Cohen, N. J. (2019). Structural and Functional MRI Evidence for Distinct Medial Temporal and Prefrontal Roles in Context-dependent Relational Memory. *J Cogn Neurosci, 31*(12), 1857-1872. doi:10.1162/jocn_a_01454

Schwarb, H., Johnson, C. L., McGarry, M. D. J., & Cohen, N. J. (2016). Medial temporal lobe viscoelasticity and relational memory performance. *Neuroimage, 132*, 534-541. doi:10.1016/j.neuroimage.2016.02.059

Shackleford, D. M., & Jamsen, K. M. (2016). Quantifying Uncertainty in the Ratio of Two Measured Variables: A Recap and Example. *Journal of Pharmaceutical Sciences, 105*(11), 3462-3463. doi:https://doi.org/10.1016/j.xphs.2016.07.019

Sinkus, R., Siegmann, K., Xydeas, T., Tanter, M., Claussen, C., & Fink, M. (2007). MR elastography of breast lesions: understanding the solid/liquid duality can improve the specificity of contrast-enhanced MR mammography. *Magn Reson Med, 58*(6), 1135-1144. doi:10.1002/mrm.21404

Solamen, L. M., McGarry, M. D., Tan, L., Weaver, J. B., & Paulsen, K. D. (2018). Phantom evaluations of nonlinear inversion MR elastography. *Physics in Medicine & Biology, 63*(14), 145021. doi:10.1088/1361-6560/aacb08

Streitberger, K.-J., Sack, I., Krefting, D., Pfüller, C., Braun, J., Paul, F., & Wuerfel, J. (2012). Brain Viscoelasticity Alteration in Chronic-Progressive Multiple Sclerosis. *PLOS ONE, 7*(1), e29888. doi:10.1371/journal.pone.0029888

Takamura, T., Motosugi, U., Sasaki, Y., Kakegawa, T., Sato, K., Glaser, K. J., . . . Onishi, H. (2020). Influence of Age on Global and Regional Brain Stiffness in Young and Middle-Aged Adults. *J Magn Reson Imaging, 51*(3), 727-733. doi:10.1002/jmri.26881

Tan, L., McGarry, M. D., Van Houten, E. E., Ji, M., Solamen, L., Weaver, J. B., & Paulsen, K. D. (2017). Gradient-Based Optimization for Poroelastic and Viscoelastic MR Elastography. *IEEE Trans Med Imaging, 36*(1), 236-250. doi:10.1109/tmi.2016.2604568

van Dommelen, J. A. W., van der Sande, T. P. J., Hrapko, M., & Peters, G. W. M. (2010). Mechanical properties of brain tissue by indentation: Interregional variation. *Journal of the Mechanical*

Behavior of Biomedical Materials, 3(2), 158-166. doi:https://doi.org/10.1016/j.jmbbm.2009.09.001

Van Houten, E. E., Paulsen, K. D., Miga, M. I., Kennedy, F. E., & Weaver, J. B. (1999). An overlapping subzone technique for MR-based elastic property reconstruction. *Magn Reson Med, 42*(4), 779-786. doi:10.1002/(sici)1522-2594(199910)42:4<779::aid-mrm21>3.0.co;2-z

Van Houten, E. E., Weaver, J. B., Miga, M. I., Kennedy, F. E., & Paulsen, K. D. (2000). Elasticity reconstruction from experimental MR displacement data: initial experience with an overlapping subzone finite element inversion process. *Medical physics, 27*(1), 101-107. doi:10.1118/1.598861

Wuerfel, J., Paul, F., Beierbach, B., Hamhaber, U., Klatt, D., Papazoglou, S., . . . Sack, I. (2010). MR-elastography reveals degradation of tissue integrity in multiple sclerosis. *Neuroimage, 49*(3), 2520-2525. doi:https://doi.org/10.1016/j.neuroimage.2009.06.018

Zienkiewicz, O. C., Taylor, R. L., Nithiarasu, P., & Zhu, J. Z. (1977). *The finite element method.* (Vol. 3): London: McGraw-Hill.